Effect of geometry variation on the mechanical behavior of the proximal femur

Amirhossein Borjali[1], Mahdi Mohseni[1], Su Mei Van[2], Mahmoud Chizari[3*]

[1] Mechanical Engineering Department, Sharif University of Technology, Tehran, Iran
[2] School of Engineering, University of Aberdeen, Aberdeen, UK
[3] School of Engineering and Computer Science, University of Hertfordshire, Hatfield, UK

ABSTRACT:

The mechanical behavior of a proximal femur under a normal body weight loading was examined. The geometry of the proximal femur was created in a finite element model using 29 reference points measured on the CT scan images of a patient. Four additional sets of measurements were calculated using ±(1) and ±(2) the standard deviation of the original set and the result of models was compared. The stress distribution and the locations of critical normal and shear stress, as well as the effect of the femur geometry which may be most susceptible to failure were examined. The findings of this study demonstrate an inferior distribution of stress in the plus-standard deviation models and indicate less ability to bear weight. The minus-standard deviation models appear to be better suited to bearing weight and indicate a more even distribution of the stresses generated within the proximal femur.

Keywords: finite element analysis, geometry, proximal femur, standard deviation, stress distribution

1. INTRODUCTION

The evolution of a human into an upright, two-legged being has led to the hip and lower limbs becoming the chief weight-bearing structures. Activities such as running and jumping involve high impact forces that generate further stress in the bones of the lower limb, in addition to those caused by the load of normal body weight. [1]

The femur serves as a powerful lever, transmitting large magnitudes of load essential to everyday movement. It is the largest and longest bone and in the human body [2] and can be divided into the diaphysis (shaft) and the articular surfaces at each end.

The shaft of the femur is basically a tubular structure made up of a thick layer of dense, compact bone tissue (cortical bone) that surrounds a hollow cavity known as the medullary cavity. Towards the proximal femur, the thickness of the cortical bone quickly decreases. The space within the proximal femur is replaced by cancellous bone arranged in a complex lattice structure, known as the trabeculae. The trabeculae can be divided into two systems: the principal compression system and the principal tension system. [2, 3]

Studies on the femur have been made that show an overall compression in the bone [4, 5]. Rudman et al. [6] go a step further to examine the stress distribution in the proximal, where they hypothesize that the proximal femur is mainly in compression under physiological loading, and their results support this hypothesis. The pattern of compression and tension stresses have been separated on proximal femur as seen in Fig. 1.

* E-mail address: Mahmoud.Chizari@yahoo.com

The objective of this study is to create a simulation based on the model done by Rudman et al. [6]. However, as the geometry and material properties (such as the apparent density of bone tissue) of the femur may change due to age, nutritional status or bone disease. The ensuing study examines how the stress distribution in the proximal femur may change when its geometry altering. It will also attempt to identify the locations of maximum normal and shear stress, as well as the areas and geometries, which may be most susceptible to failure.

2. MATERIAL AND METHODS

To address hypothesis of the current study, the proximal femur's CT scan data of a single individual was used. All personal information of the patient including gender and age remained undisclosed. A set of references with twenty-nine nodes were specified on the proximal femur for a coordinate geometry and subsequent measurements. The original model was built base based on this coordinate geometry and called (0)-model. Four additional sets of measurements were calculated using ±(1) and ±(2) the standard deviation of the original set. Abaqus CAE (Simulia Dassault Systèmes, US) finite element (FE) software was used to build and analyze the simulation models. The resulting models are named according to their deviation from the original model ((0)-model). In total, 5 models (0, -1, -2, +1 and +2 models) created and were used in the ensuing study.

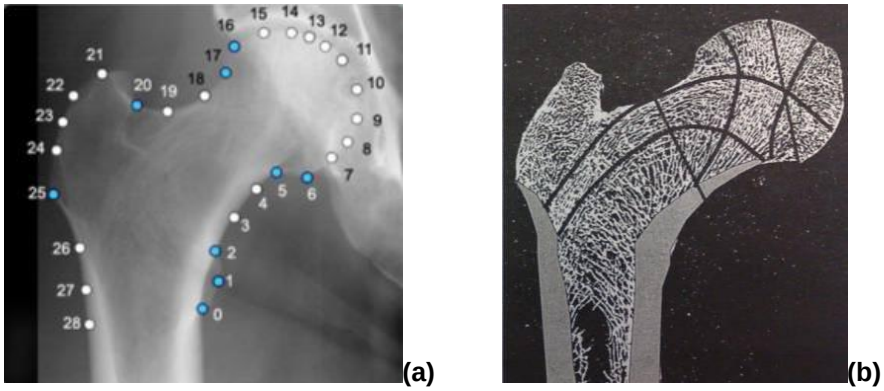

Fig. 1. Coordinate geometry for the proximal femur (Provided by the Division of Applied Medicine, University of Aberdeen) (a); pattern of trabeculae within proximal femur [6] (b).

For all the models, the bone is partially reconstructed. The model includes a representative section of the acetabulum and labeled "H4" (Fig. 2). The distal femur that includes the knee area has been excluded in the modeling. For stability and more accurate rendering of the bone's deformation under loading, an arbitrary length of the shaft is included. The cortical bone surrounding the femoral shaft is assigned a density of 2.2 g/cc [7], Young's modulus of 17GPa, and Poisson's ratio of 0.33 [4, 6].

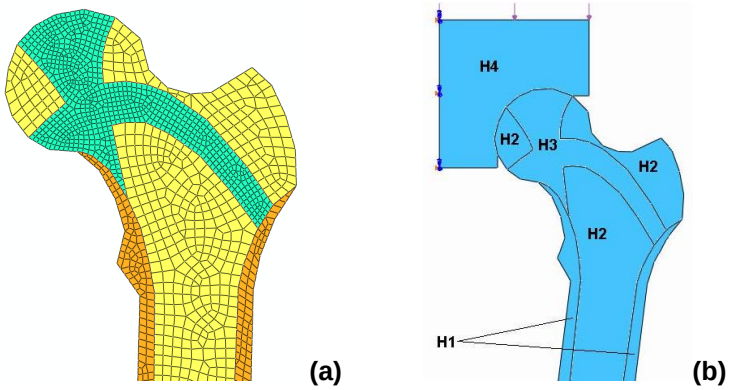

Fig. 2. The finite element model created based on the measured geometry and proposed pattern of the proximal femur (a); partition of the proximal femur based on the pattern of tension-compression presented in Fig 1 (b).

The internal structure of the models is partitioned (Fig. 2), as defined by Rudman et al. [6], following the lines of stress in the bone trabeculae. The principal compression and principal tension groups (Fig. 1) are represented as a single part labeled "H3" in the FE model (Fig. 2). This part was given Young's modulus of 400MPa. [6] Density and Poisson's ratio

remains the same as the cortical bone. The remaining surrounding trabeculae and cavity in the shaft (H2) are given a modulus of 100 MPa [6] and apparent density of 1.2 g/cc from a range of values. [8] The acetabulum is assigned the same material properties as the H3 trabeculae. Each part is assumed to be of homogeneous and isotropic material. Although true bone trabeculae have a lattice structure, it is challenging to recreate precisely. The assumptions should give a close enough representation and fairly good results [4, 5, 6, 9], in addition to making the simulations more comfortable to work with.

The model is meshed using 4-node quadrilateral elements with reduced integration. As a 2-dimensional model, no thickness is assigned, and the model only undergoes linear plane stress in two directions. A finer mesh is assigned in the H3 part in order to obtain more precise results in the proximal femur.

Boundary conditions are applied to replicate in vivo conditions as closely as possible (Fig 3). Part H4 is fixed only on the medial side. The distal end is pinned, as there should be zero-moment at the knee when weight is applied. The average body weight of 700N (70kg) is assumed. Further, assuming that bodyweight is uniformly distributed during the two-legged standing stance (the person is standing at rest), it is inferred that the load carried by each leg is 350N.

3. RESULTS AND DISCUSSION

3.1 Deformation and displacement

When the load was applied, the models showed a deflection on the femoral head, together with a displacement in the lateral direction in by femoral shaft. These were the maximum displacements in the entire represented femur, and the location of these deflections remained unchanged throughout all models. The values of these displacements are shown below in Table 1.

Table 1. Maximum displacement (mm) values found in the femoral head and shaft

Standard deviation	-2	-1	0	+1	+2
Displacement, femoral head	21.5	20.0	19.0	18.0	12.0
Displacement, shaft	26.9	25.0	24.8	23.0	17.0

Fig. 3 shows a typical femur model after the load was applied. Except for the case of the (+2)-model, the readings show displacement differing by about ±2.0mm from the (0)-model, which does not seem too unusual. The (+2)-model is the exception with an uncharacteristically large variance in values. With this in mind, we carry on examining the normal and shear stress responses of the (0)-model and the standard deviation models.

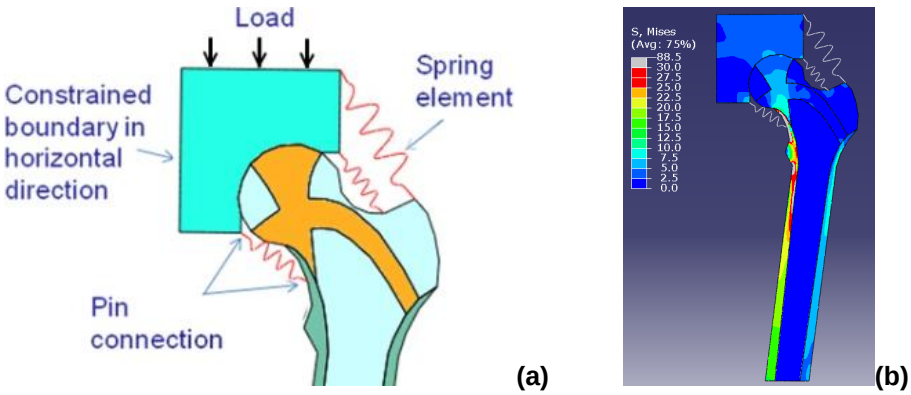

Fig. 3. (a) loading and boundary conditions; (b) a typical stress distribution in an analyzed model. The colors show the level of stress on the bone.

3.2. Normal & shear stress response

3.2.1. Mean/average model, (0)-model

Under the static 350N load, the bulk of the trabeculae is shown to be under stresses up to -1.1 kN/cm^2. A contour plot of normal stress reveals an area in part H3 under higher compression. The compression in this area appears to stem from the acetabulum and continues directly into the cortical bone of the medial shaft, which is under even higher compressive stress. The compression in the proximal femur is most concentrated at a point in the superior head, with a value of -6.4kN/cm^2. Maximum tensile stress in the proximal femur is output as +1.6kN/cm^2 and is in a mesh element directly below the maximum compression.

The output readings from the model show that the femur is mainly under negative shear stress. Negative shear found in the proximal femur and acetabulum appears to be of relatively low magnitude, and the plot shows areas in the acetabulum and the inferior femoral head that reach values up to -0.6kN/cm^2 to -0.94kN/cm^2. This is about three times of values found in the surrounding trabeculae.

The largest shear values in the proximal femur are in the superior femoral head. The maximum negative shear is determined to be -1.7kN/cm^2 and is accompanied by a mesh element bearing the maximum positive shear (+1.8kN/cm^2) in the same part.

3.2.2. Minus one (-1) standard deviation model

The (-1)-model shows the trabeculae to be under compressive stresses between -0.88kN/cm^2 to -2kN/cm^2, the contour plot appearing to suggest a more uniform distribution of stresses. The large area of higher compression in the femoral head, as seen during the (0)-model simulation, does not appear in the plot for the (-1)-model. However, there is evidence that a similar pattern of behavior may emerge. The result shows a small cluster in the inferior femoral neck in a higher range of compression than its surroundings; this connects to the medial cortical bone that is also in comparatively high compression. The maximum compression in the proximal femur is also shown to be in the superior femoral head, although it is smaller in magnitude at -6.0kN/cm^2.

Within the greater trochanter, the trabeculae appear to be in mild tension. The H3 part trabeculae experience a principal tensile load and show tension growing towards the lateral metaphysis. The maximum tension (+1.1kN/cm^2) in this model is found here and is located right next to the cortical bone.

The metaphysis experiences relatively low positive shear. The most significant positive shear stress (+0.34kN/cm^2) found in the femoral neck is in the inferior, close to the cortical bone.

The negative shear found in this model mostly follows a similar trend of being relatively small in magnitude. The trend breaks in the most inferior and superior sections of the head. The inferior femoral head shows negative shear stress in the region of -1.0kN/cm^2 building up where the cortical bone starts to grow thicker. The superior proves to be the location of both the maximum negative and maximum positive shear stresses. The values of which are -1.3kN/cm^2 and +1.6kN/cm^2, and their location corresponds to the location of maximum compression. The proximal femur is ultimately found to be under net negative shear stress.

3.2.3. Minus two (-2) standard deviation model

The normal stress result of (-2)-model bears a close resemblance to the corresponding plot for the (-1)-model. In most of the trabecular bone, the model registers compression values up to around -0.9kN/cm^2 to -1.8kN/cm^2. Like the (-1)-model, there is an area in the inferior neck under higher compression leading into the cortical bone of the medial shaft. The point of maximum compressive stress in the superior head is found to be -5.6kN/cm^2.

The maximum tension in the proximal femur is located in the lateral metaphysis and within the H3 part, similar to that seen in the (-1)-model. The magnitude is also around +1.1kN/cm^2.

The result of shear stress for the (-2)-model shows most of the metaphysis to be under low positive shear stress, with a maximum of +0.4kN/cm2 found in the inferior neck, close to the cortical bone. Negative shear stress occurs in the epiphysis, mainly in the inferior and medial. The maximum negative shear for the proximal femur is -1.4kN/cm^2, which is found in the inferior femoral head. The location of maximum negative shear is different from the other models, virtually on the opposite side. The maximum positive shear in the head reaches just under +1.0kN/cm^2, and its location remains unchanged from other models. Negative shear is still generated next to this point but remains relatively low in magnitude (-0.36kN/cm^2).

Despite large areas of the proximal femur being under positive shear, the magnitudes are very low in comparison to the small areas that are under much higher magnitudes of negative shear stress. This results in the proximal femur being under net negative shear.

3.2.4. Plus (+1&+2) standard deviation models

The result of the normal stress in the (+1)-model looks almost identical to the (0)-model. The values in the field output report of normal and shear stress indicate a shift towards tensile stress in the proximal femur. Despite this shift, the field output shows that the net stress response in the proximal femur remains compressive and smaller in magnitude than the (0)- model.

The location of maximum compression in the proximal femur remains in the superior femoral head and is found to be -7.7kN/cm^2. This turned out to be the highest compression reading out of all the five models. In addition, the maximum tensile stress (+2.5kN/cm^2) in the proximal femur was found to be located close to the maximum compression. This is like what was seen in the (0)-model response.

The shear stress for this model also bears a substantial similarity to the (0)-model. The same areas have been highlighted, although as with the normal stress response, the values show a fair amount of difference. The data extracted show the magnitudes of both negative and positive shear increasing in the proximal femur. Despite this, the net shear remains negative and is of lower magnitude. As well, part H3 demonstrates a net positive shear, although its value is comparatively small.

The maximum negative and positive shear values (-2.4kN/cm^2; +2.1kN/cm^2) are found in the superior femoral head, as with the (0) & (-1)-models. Similarly, besides being close in proximity to each other, these maximum shear stresses coincide with the location of the maximum normal stresses.

The normal stress output values for the (+2)-model show it has the lowest range of response of the five models. Most of the proximal femur is found to bear stresses of about -0.6kN/cm^2 to just below +1.0kN/cm^2.

This model continues to exhibit higher compression areas in the femoral head that continue into the cortical bone. The result can be said to look most like the (-2)-model. There is no change in the location of the maximum compressive and maximum tensile stresses of the proximal femur and in its superior epiphysis. However, the maximum compression decreases dramatically to -6.1kN/cm^2, falling below the (0)-model. The maximum tension is output as +2.3kN/cm^2.

The shear stress result of the (+2)-model seems closer to those of the minus deviation models. It clearly shows positive shear building up in the metaphysis (particularly nearer the greater trochanter).

The position of maximum shear in the proximal femur remains unchanged and is found in the superior head within part H3. The maximum negative shear is found to be -2.0kN/cm^2, and the maximum positive shear is +1.7kN/cm^2. Despite the negative shear having a higher magnitude, the proximal femur for this model ends up being in net positive shear, in part due to a larger existence of high magnitude positive shear in part H3. In addition, it was found that the location of maximum negative shear in the H2 part has migrated. In previous models, this point was in the superior femoral head, next to the maximum shear stresses of the entire proximal femur. In the (+2)-model, this migrates through the H2 part into the distal femoral shaft.

4. DISCUSSION

The degree to which the femoral head deflects downward (Table 1) resembles the findings of a previous study. [4] In our case, the readings do not appear unusual until the (+2)-model. The minus-models demonstrate gradually increasing displacement. The plus-models were thus expected to show similar behavior of gradual decrease in displacement. Although the plus-models do show smaller displacements, the (+2)-model shows a sharper decrease in magnitude despite the same amount of load. Considering the behavior of previous models and the shifts in external geometry, the (+2)-model appears to show less flexibility. This behavior may be indicative of anisotropic nature. It suggests that this study's assumption that bone tissue is isotropic may be over-simplistic. While the isotropic material assumption can be useful, it seems to only be applicable to a certain extent and is unlikely to give genuinely accurate results.

The results consistently show in all models that the proximal femur is under net compression during loading. The part H3 carries higher compressive stresses that are transmitted into the cortical bone, and that are consistent with the location of the principal compression system in the trabeculae. This coincides with the findings of Rudman [6]. The simulations

conducted in this study also reveal the maximum point compression in the proximal femur is always located at a point in the superior head and is generated within the compression system in part H3.

The maximum values of compressive, tensile, and shear (negative and positive) stress found in the entire proximal femur of each model are shown in Table 2. In each case, the maximum is generated within the H3 trabeculae and almost always found to occur in the same location of the superior femoral head. Exceptions are seen in the minus-models, where the different locations are identified in square parentheses.

Table 2. Maximum normal & shear stress values in the proximal femur

Standard deviation model	**-2**	**-1**	**0**	**+1**	**+2**
Compression, kN/cm^2	-5.6	-6.0	-6.4	-7.7	-6.1
Tension, kN/cm^2	+1.1	+1.1	+1.6	+2.5	+2.3
Negative shear stress, kN/cm^2	-1.4	-1.3	-1.7	-2.4	-2.3
Positive shear stress, kN/cm^2	> +1.0	+1.6	+1.8	+2.1	+1.7

The output report from Abaqus shows net compression in the proximal femur decreasing through the models, gradually at first from the (-2)-model to the (0)-model. The decrease is sharper from the (0)-model onwards. The (+2)-model shows net compression values in the proximal femur that are between 2-3 times smaller than the (0)-model.

From the values in Table 2 and the output report, it appears that the proximal femur becomes more capable of distributing stress loads internally as the external geometry shifts towards a lower deviation. Although, net compression is higher, the maximum compressive load decreases, and the position of maximum tension shifts from the medial to the lateral proximal femur.

In theory, the opposite should then be right in the plus-standard deviation models. This does happen in the (+1)-model, although to a much higher degree than expected. This hypothesis then fails in the (+2)-model. The maximum tension remains relatively high, and like its two immediate predecessors, it is located right next to the point of maximum compression. However, the maximum compressive load itself suddenly decreases, along with net compression values. As with the differences in displacement, this atypical behavior points towards an anisotropic characteristic and casts doubt on the assumption of linear elasticity. The sudden difference in readings from the (+2)-model may suggest that the model is less reliable under the current simulation. Also constant in the simulated models are the locations of the resultant maximum negative and positive shear stress in the proximal femur. The results show the locations of the maximum shear stresses (both negative and positive) coincide with the location of maximum compressive stress in the proximal femur. The (-2)-model is the exception, whereby the maximum negative shear, in this case, is found in the inferior femoral head instead of the superior. This area is also highlighted in the other models as a location subject to higher negative shear than the surrounding trabecular bone in the inferior epiphysis. Except for the (+2)-model, the simulations show net negative shear stress generated in the proximal femur.

The plus-models show larger values of shear, and the output report shows that in both cases, the trabecular bone within part H3 is under net positive shear. The magnitude is relatively low in the (+1)-model but is shown to be much higher in the (+2)-model. Extraction of the maximum shear values from part H2 and their locations in each model provide a better understanding of these behaviors. This is tabulated in Table 3.

Table 3. The maximum shear stresses in part H2

Standard deviation	**-2**	**-1**	**0**	**+1**	**+2**
Negative shear stress, kN/cm^2	-0.36	-0.40	-0.36	-0.37	-0.21
Positive shear stress, kN/cm^2	+0.40	+0.34	+0.34	+0.37	+0.26

In all cases, the maximum positive shear within this part is in the inferior femoral neck, near where the cortical bone starts to thicken. A maximum negative shear is found in the superior head, close to the location of the maximum positive shear of the H3 part trabeculae. The (+2)-model is an exception. In this model, the maximum negative shear in the H2 part migrates from the trabeculae into the shaft. Presumably, the area made up of the medullary cavity.

This migration and the readings recorded in Tables 2 & 3 could imply that in this model, (i) some form of failure has occurred under the current simulated conditions or (ii) the femoral shaft has now become at risk of failure for the particular geometry. If failure is indeed the case, it is highly likely to have occurred in the superior femoral head.

Overall, the findings in this study demonstrate the poorer distribution of stress by the plus-standard deviation models and seem to indicate that these have a weaker ability to bear weight. On the other hand, the minus-standard deviation models seem better suited to bearing weight and indicate a more even distribution of the stresses generated within the proximal femur.

Failure in the proximal femur seems most likely to occur in the superior femoral head, as the location of maximum compression remains in this area throughout each of the simulated models. The (0)-and plus-models seem particularly at risk since this is the location of maximum tension in these models as well. For the most part, the same can be said of the maximum shear stresses found in each model. The (-2)-model may seem to be an exception to the rule since the maximum negative shear shifts down to the inferior head and is no longer acting directly against the maximum positive shear. However, it continues to lie along the principal compression system of the trabecular bone that appears to transmit stress into the cortical bone. This may lead to failure that starts from the inferior head rather than the superior. This observation may be supported by the presence of some higher compression and negative shear in this region throughout all five models.

The model used in this study is a basic 2-dimensional representation of the femur. Currently, the study does not consider the forces generated by ligaments and the muscle surrounding the femur. It also excludes the effects of the articular cartilage and synovial fluid that lies between the acetabulum and femoral head. The inclusion of these factors in future studies will give a much more accurate rendition of results.

With a 2-dimensional model, the study can give a good approximation as to the behavior of the proximal femur under loading but cannot be truly accurate. A 3-dimensional model, especially one that includes the physiological factors mentioned above, may give a better representation.

The trabecular bone in the proximal femur is a complicated mesh of lamellar bone tissue. The exact architecture is difficult to determine and even more challenging to represent in a computer simulation, not to mention one that is only in 2-dimensions. Furthermore, the findings of this study, looking at spread of forces across the different models imply an anisotropic behavior in bone tissue. This suggests that to avoid structural failure, the in vivo bone will adjust itself to deal with the range of applied loading and the varying stresses generated within the femur [12, 13]. This supports Wolff's law, which states that bone is laid down in response to the quantity and quality of the load experienced [3, 4, 10]. Future simulations may have to take this adaptive remodeling into account.

5. CONCLUSIONS

The finite element simulations reveal the presence of more considerable compression and tension in the trabeculae that were consistent with the areas defined as the principal compression and principal tension systems. The findings of this study support the theory that trabecular bone in the proximal femur acts as a vehicle to transfer the bulk of the stress borne by the femur into the more compact and dense cortical bone. The path of transmission is consistent with the lines of stress previously found by other researchers [3, 11].

We see that when the load is applied, a similar pattern of deformation occurs (downwards on the femoral head and outward in the direction of the femoral shaft), though of varying magnitude.

Interestingly, we have also located the presence of increased shear response in the superior aspect of the femoral head and the inferior neck. These areas may contribute to structural failure in the proximal femur, such as in predisposition to fractures, especially in cases where there is a decrease in bone density or repetitive injury.

The findings of this study suggest that bone is anisotropic in nature; and that the structure of trabecular bone within the proximal femur may change with outer geometry or loading conditions.

ACKNOWLEDGMENTS

The original model ((0)-model) used in this study was based on the CT scans of a single individual provided by the Division of Applied Medicine, University of Aberdeen. Their support during this study is highly appreciated.

COMPETING INTERESTS

Authors have declared that no competing interests exist.

AUTHORS' CONTRIBUTIONS

We attest to the fact that all authors listed on the title page have contributed significantly to work, have read the manuscript, attest to the validity and legitimacy of the data and its interpretation, and agree to its. All authors read and approved the final manuscript.

CONSENT (WHERE EVER APPLICABLE)

No manuscripts will be peer-reviewed if a statement of patient consent is not presented during submission (wherever applicable).
This section is compulsory for medical journals. Other journals may require this section if found suitable. It should provide a statement to confirm that the patient has given their informed consent for the case report to be published. Journal editorial office may ask the copies of the consent documentation at any time.

Authors may use a form from their own institution or SDI Patient Consent Form 1.0. It is preferable that authors should send this form along with the submission. But if already not sent during submission, we may request to see a copy at any stages of pre and post publication.

If the person described in the case report has died, then consent for publication must be collected from their next of kin. If the individual described in the case report is a minor, or unable to provide consent, then consent must be sought from their parents or legal guardians.

Authors may use the following wordings for this section: "All authors declare that 'written informed consent was obtained from the patient (or other approved parties) for publication of this case report and accompanying images. A copy of the written consent is available for review by the Editorial office/Chief Editor/Editorial Board members of this journal."

ETHICAL APPROVAL (WHERE EVER APPLICABLE)

All authors hereby declare that "Principles of laboratory animal care" (NIH publication No. 85-23, revised 1985) were followed, as well as specific national laws where applicable. All experiments have been examined and approved by the appropriate ethics committee.

REFERENCES

[1] S. Liong and R. Whitehouse, "Lower extremity and pelvic stress fractures in athletes," *The British journal of radiology,* vol. 85, pp. 1148-1156, 2012.

[2] S. J. Allison, J. P. Folland, W. J. Rennie, G. D. Summers, and K. Brooke-Wavell, "High impact exercise increased femoral neck bone mineral density in older men: a randomised unilateral intervention," *Bone,* vol. 53, pp. 321-328, 2013.

[3] I. G. Jang and I. Y. Kim, "Computational simulation of simultaneous cortical and trabecular bone change in human proximal femur during bone remodeling," *Journal of Biomechanics,* vol. 43, pp. 294-301, 2010.

[4] S. Nawathe, B. P. Nguyen, N. Barzanian, H. Akhlaghpour, M. L. Bouxsein, and T. M. Keaveny, "Cortical and trabecular load sharing in the human femoral neck," *Journal of biomechanics,* vol. 48, pp. 816-822, 2015.

[5] M. M. Juszczyk, L. Cristofolini, and M. Viceconti, "The human proximal femur behaves linearly elastic up to failure under physiological loading conditions," *Journal of biomechanics,* vol. 44, pp. 2259-2266, 2011.

[6] K. E. Rudman, R. M. Aspden, and J. R. Meakin, "Compression or tension? The stress distribution in the proximal femur," *BioMedical Engineering OnLine* vol. 5, p. 12, Feb 2006.

[7] D. C. Wirtz, N. Schiffers, T. Pandorf, K. Radermacher, D. Weichert, and R. Forst, "Critical evaluation of known bone material properties to realize anisotropic FE-simulation of the proximal femur," *Journal of biomechanics,* vol. 33, pp. 1325-30, Oct 2000.

[8] R. Oftadeh, M. Perez-Viloria, J.C. Villa-Camacho, A. Vaziri, A. Nazarian, "Biomechanics and mechanobiology of trabecular bone: a review," *Journal of biomechanical engineering*, vol. 137,1, 2015. doi:10.1115/1.4029176.

[9] D. Nolte, A.M.J. Bull, "Femur finite element model instantiation from partial anatomies using statistical shape and appearance models, *Medical Engineering & Physics*, vol. 67, pp. 55-65, 2019.

[10] J.F. Fetto, "A Dynamic Model of Hip Joint Biomechanics: The Contribution of Soft Tissues, ". *Adv Orthop*. 5804642, 2019. doi:10.1155/2019/5804642.
[11] I.G. Jang, I.Y. Kim, "Computational study of Wolff's law with trabecular architecture in the human proximal femur using topology optimization." *Journal of Biomechanics*, vol. 41, pp. 2353-2361. 2008.
[12] M. Athapattu, A.H. Saveh, S.M. Kazemi, B. Wang, M. Chizari, "Measurement of the femoral head diameter at hemiarthroplasty of the hip," *Procedia Technology,* vol. 17, pp. 217–222, 2014. doi: 10.1016/j.protcy.2014.10.231.
[13] R. Suppanee, M. Yazdifar, M. Chizari, I. Esat, N.V. Bardakos, R.E. Field, "Simulating osteoarthritis: the effect of the changing thickness of articular cartilage on the kinematics and pathological bone-to-bone contact in a hip joint with femoroacetabular impingement," *Eur Orthop Traumatol*, vol. 5, pp. 65-73, 2014. doi: 10.1007/s12570-013-0196-0.